Second International Conference on
Microchannels and Minichannels (ICMM2004)
June 17–19, 2004, Rochester, New York USA
ICMM2004-2404

HIGH FREQUENCY AC ELECTROSPRAYING OF DIELECTRIC LIQUIDS

Leslie Y. Yeo, Dimitri Lastochkin and Hsueh-Chia Chang[1]

Center for Microfluidics and Medical Diagnostics
Department of Chemical and Biomolecular Engineering
University of Notre Dame, Notre Dame, IN 46556, USA
[1] E-mail: hchang@nd.edu

ABSTRACT

A new high-frequency (> 10 kHz) AC electrospray phenomenon which behaves distinctly to DC electrosprays is investigated. Unlike DC electrosprays, the drops do not emanate from the usual well-defined Taylor cone-jet and carry no net charge. Instead, the meniscus vibrates at a resonant frequency associated with its capillary-inertia vibration time, periodically ejecting drops with dimensions of order 10 μm under the action of the Maxwell-Wagner electric stress at the meniscus tip. Above a crossover frequency, the polarization and direction of the Maxwell force reverses and an apparent electrowetting effect is observed. A simple lubrication model is used to generate spatio-temporal evolution profiles for the stretched liquid meniscus tip as a function of the Maxwell-Wagner stress and a capillary number. From a self-similar scaling technique, the meniscus is shown to advance as $t^{1/2}$.

INTRODUCTION

Electrospraying, which is otherwise known as electrohydrodynamic atomization, is a very useful technique that employs the principle of electrostatic charging to generate very small liquid aerosol drops. By applying a high voltage across a micro-needle and a ground electrode, Maxwell electric stresses give rise to a stretched meniscus tip at the needle orifice which eventually pinches-off to form an aerosol drop. In DC electrospraying, the drops produced carry excess charge of the same sign thereby creating a vast potential for its use as a 'soft' ionization technique for the generation of gas phase ions of complex and non-volatile biological molecules in mass spectrometry (Fenn et al., 1989). As such, electrosprays are now being used to a vast extent in genomics, proteomics and drug discovery.

By applying a high frequency AC source (10–280 kHz) in place of the DC power supply in the electrospraying of a dielectric liquid, we demonstrate a new phenomenon driven by Maxwell-Wagner interfacial polarization and capillary resonance (Yeo et al., 2004). The micron sized drops produced are distinct in size to that in DC electrospraying and carry no net charge. Moreover, the drops are not ejected from a well-defined Taylor cone, which is characteristic in stable DC electrospray modes. These different attributes therefore create a wider spectrum of technological possibilities for electrospray applications. We anticipate that the electroneutral drops generated from the AC electrospray will find huge commercialization potential in drug delivery systems such as inhalers for diabetic and asthma patients. Furthermore, the negligible current and hence power requirement will allow the technology to be miniaturized to portable dimensions.

EXPERIMENTS & SCALING THEORY

The experiments were performed by passing a high voltage AC power supply generated by a function/arbitrary waveform generator (HP 33120A), RF amplifier (Powertron 250 A 10 Hz–1 MHz) and high voltage output transformer (Industrial Test Equipment) across a metal hub micro-needle (Hamilton N733) and ground electrode consisting of a strip

of copper tape. This is illustrated in Fig. 1. The micro-needle, filled with 95% ethanol (AAPER Alcohol & Chemical Co. 190 Proof), properties of which can be found in Table 1, had an outer diameter of 0.21 mm and a thickness of 0.05 mm, and was mounted at a 50° angle inclination to the horizontal. The separation distance between the needle tip and the ground electrode was 5 mm. The imaging equipment comprised of a high speed video camera (Kodak Ektapro 1000 Imager and High-Spec Processor) connected to a telescopic lens which provided 800x overall magnification and a fibre-optic lamp (Fiber-Lite PL-800) to provide background lighting. The images were recorded at rates of 1000 and 6000 fps.

The distinction of the electrospray behaviour in our observations with that of DC electrosprays was immediately evident. None of the DC electrospray modes, namely, the dripping, microdripping, spindle, intermittent-jet, simple-jet, cone-jet, and ramified-jet modes (Clopeau and Prunet-Foch, 1990; Grace and Marijnissen, 1994) were observed. In particular, we note the absence of a well-defined conical meniscus with a half-angle approximately equal to the 49.3° Taylor angle, known as the Taylor cone, which is characteristic of the stable cone-jet mode in DC electrosprays. Instead, the meniscus vibrated at a resonant frequency f_1 of order 10 Hz and periodically ejected drops at the same frequency or at some higher frequency f_2, of order 1 kHz. The drops appeared to be electroneutral as their flight paths did not follow the field lines and were easily deflected by cross flow. This is in contrast to the drops generated by DC electrosprays which possess a net charge. In addition, the ejected drops, approximately 10 μm in diameter, are larger than those generated in DC electrosprays. This is perhaps a consequence of the electroneutrality of the drops. The small sizes of the charged drops produced in DC electrosprays are a result of the disintegration of the ejected drop into several smaller droplets when the Rayleigh limit of coulombic fission is exceeded, i.e. when the repulsion of the like charges within the drop overcomes the surface tension holding the drop together. The drops produced in the AC electrospray, however, do not undergo such disintegration due to their electroneutrality, thus explaining their larger dimensions. On the contrary, drops are produced by a viscous or inertial pinch-off mechanism which we attribute to the flow induced by normal Maxwell stresses and further compounded by the resonant oscillation of the drop. We will discuss these mechanisms in further detail in a later section.

Table 1. Physical properties of 95% Ethanol

Physical property	Approximate value
Interfacial tension, γ_L	~ 25 mN/m
Liquid density, ρ_L	~ 816 kg/m^3
Liquid viscosity, μ_L	~ 1.2 mPa s
Liquid conductivity, κ_L	~ 4 x 10^{-5} S/m
Liquid permittivity, ε_L	~ 2.15 x 10^{-10} F/m

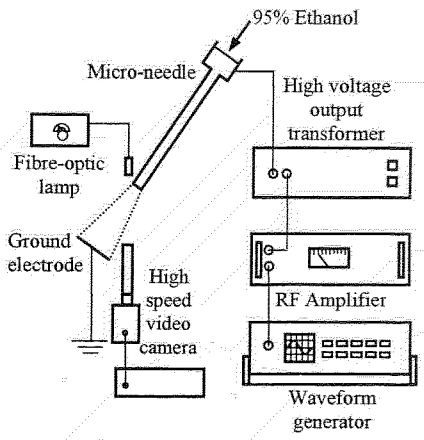

Fig. 1 Experimental apparatus.

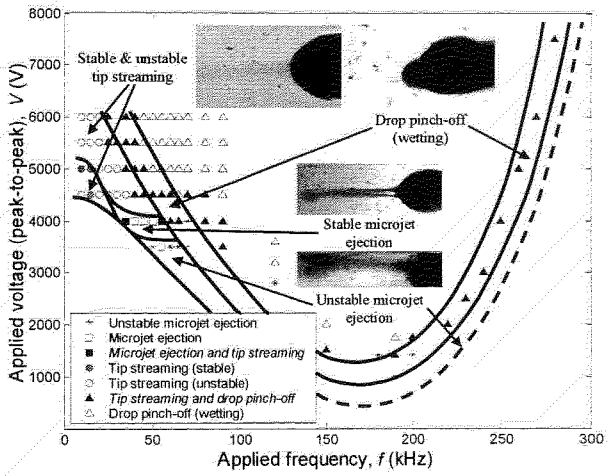

Fig. 2 Pattern map indicating the various electrospray modes in which drop ejection is confined to a voltage belt.

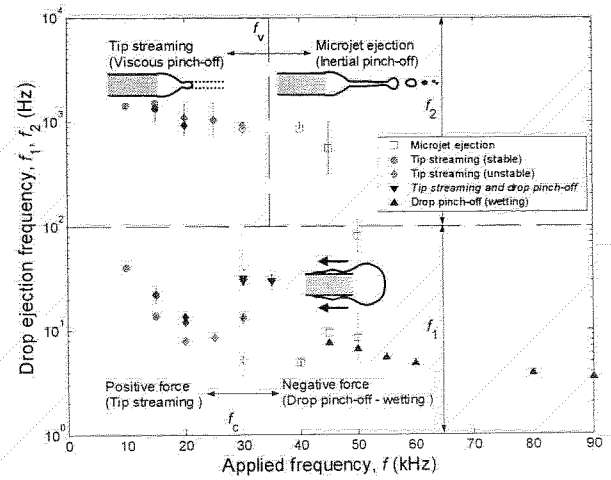

Fig. 3 Drop ejection frequencies f_1 and f_2 as a function of the applied frequency f.

From our observations, it is possible to categorize several AC electrospray modes. These are shown in Fig. 2 as a function of the applied peak-to-peak voltage V and the applied frequency f. Drop ejection is limited to a voltage belt which varied with f. Below this belt, drops were not ejected as there was insufficient electrical stress to overcome the capillary force. Above the belt, the liquid appeared to climb up the needle and suppress drop ejection. To further delineate the spray modes, we plot in Fig. 3 the drop ejection frequencies, f_1 and f_2, as a function of f by scanning across the voltage belt in Fig. 2. It can be seen that the tip streaming (Eggleton et al., 2001) mode is bi-periodic where the meniscus resonates at f_1 and intermittently ejects single or multiple drops by a tip streaming mechanism at f_2. On the other hand, drop pinch-off due to wetting effects is mono-periodic at f_1, which decreases with f as the wetting becomes more significant. The microjet ejection mode, which is peculiar to AC electrosprays, forms the boundary between the tip streaming and drop pinch-off modes. This mode appears to be bi-periodic at low f and becomes mono-periodic as f increases, i.e. when $f_2 \rightarrow f_1$. In any case, the multiple spray modes and the bi-periodic behavior seem to suggest that there is a complex interaction of various physical phenomena at different length and time scales. To provide a basic fundamental understanding of this complex behavior, we thus turn our attention to simple scaling arguments.

The Debye layer thickness λ, calculated from the conductivity of ethanol in Table 1, is approximately 0.2 μm, from which we estimate a Debye diffusion time $T_d \sim \lambda^2/D$ of 10^{-3} s. Since this is larger than the period of the applied AC field T, there is insufficient time for the Debye layer to be polarized in every half cycle of the field. Addition of trace quantities of hydrochloric acid to decrease λ did not significantly alter the quantitative behavior of the results due to the large time scale for bulk ionic diffusion R_o^2/D of 10^3 s, where $R_o \sim 5$ mm is the dimension of the drop, which is significantly greater than T. Given the above, it is unlikely that AC field-induced double layer polarization due to impurity ions in the bulk of the drop (Ramos et al., 1998) is the driving mechanism that gives rise to the Maxwell stress.

Instead, the ratio of drop viscous drainage time scales due to the double layer and Maxwell-Wagner interfacial polarization forces, $T_{DL}/T_{MW} \sim \varepsilon_o \mathrm{Re}[f_{CM}]R_o^2 E_\infty/Q \sim 10$–$100$, and $T_{MW} \sim T$ suggests that Maxwell-Wagner interfacial polarization is responsible for the Maxwell stress that stretches the meniscus tip. Here, ε_o is the permittivity of vacuum, $E_\infty \sim V/L$ where L is the electrode separation (5 mm) is the externally applied field, and, $Q \sim cN_A e R_o^3$ is the charge, where c is the ionic concentration, N_A the Avogadro constant, and e the electronic charge. The ratio of time scales above were obtained by balancing the force due to double layer polarization $F_{DL} \sim QE_\infty/R_o^2$ and the time-averaged force due to Maxwell-Wagner polarization $F_{MW} \sim \varepsilon_o \mathrm{Re}[f_{CM}]|E_\infty|^2$ with the viscous drainage force $\mu_L U/R$, where U is the characteristic velocity. f_{CM} is the Clausius-Mossotti interfacial polarization factor that allows for the influence of the angular frequency of the applied field $\omega = 2\pi f$ on the polarizability of the liquid. Allowing for a reactive current across the interface arising from gas-phase or interfacial liquid ionization, accounted for by the conductivity in the frequency domain after Fourier transformation in time, the Clausius-Mossotti factor can be written in the following Maxwell-Wagner form:

$$f_{CM} = \frac{\tilde{\varepsilon}_o - \tilde{\varepsilon}_L}{\tilde{\varepsilon}_L + 2\tilde{\varepsilon}_o}, \qquad (1)$$

where $\tilde{\varepsilon} = \varepsilon - \mathrm{i}(\kappa/\omega)$ indicates a complex permittivity.

The ratio of instantaneous charge induced by Maxwell-Wagner polarization $\varepsilon_o f_{CM} E_\infty$ to that induced by double layer polarization $\kappa_L T E_\infty$ is approximately $T_d/T \sim 10^3$–10^4 since the Debye diffusion time $T_d \sim \varepsilon_o/\kappa_L$ and since f_{CM} cannot have a value greater than 1. This lends further support for the Maxwell-Wagner interfacial polarization since double layer polarization is negligible for $f \geq 10$ Hz. We also note that the transient interfacial current inherent in the Maxwell-Wagner polarization mechanism cannot be due to bulk ion migration thus suggesting that an interfacial ionization reaction supplies the transient current that conducts across the interface.

A balance between the capillary force of the drop meniscus before application of the applied stress, which scales as $F_c \sim \gamma_L/R_o$, and the Maxwell-Wagner force F_{MW} defined above gives an estimate for the critical voltage V_c that is associated with the minimum in the lower boundary of the voltage belt, where $V_c \sim (\gamma_L L^2/\varepsilon_o \mathrm{Re}[f_{CM}]R_o)^{1/2} \sim 10^3$ V. This is in rough agreement with the minimum incipient voltage at $f \sim 180$ kHz in Fig. 2, thus lending further evidence for Maxwell-Wagner polarization as the driving mechanism giving rise to the Maxwell force that stretches the meniscus.

An important consequence if Maxwell-Wagner interfacial polarization, which arises due to the synchronized alignment of molecular dipoles within the meniscus as a result of the applied electric field and from a parallel interfacial Faradaic current, is the driving mechanism for the meniscus stretching, is that there is no net AC current resulting from the ionization reaction. Although the current due to tip polarization does produce a net charge in every half cycle of the applied field, the drop ejection frequency at f_1 is sufficiently small compared to f such that there is no net charge accumulation in the drop and hence the ejected drops are electroneutral. This is in contrast to DC electrosprays of electrolytes in which a net current is present and therefore the ejected drops possess net charge, which results in further disintegration into smaller drops due to Coulombic fission.

We now proceed to a discussion of the various drop ejection modes. In Fig. 3, drop ejection by a tip streaming mechanism was observed at low applied frequencies. As f is increased, the meniscus tip is seen to elongate into a microjet. Balancing the viscous and capillary forces defined previously, we obtain a frequency associated with the time scale for viscous-capillary drop pinch-off, $f_v \sim \gamma_L/\mu_L R_o \sim 20$–$50$ kHz, below which viscous effects become significant. f_v therefore forms the boundary between the viscous-capillary

drop pinch-off mode associated with the tip streaming mechanism and the capillary-inertia drop pinch-off mode associated with microjet formation. When $f < f_v$, increasing viscous dominance rigidifies the meniscus against further elongation and violent oscillations, thus giving rise to the stable tip streaming mode observed in Fig. 2. The number of drops ejected from the tip also increases to a maximum in this mode. It is postulated that further decreases in f will result in the recovery of the stable Taylor cone as observed by Borra et al. (1999) at low AC frequencies of 50 Hz. On the other hand, when $f > f_v$, drops are ejected intermittently from the end of a long liquid thread by a microjet break-up mechanism. As the capillary-inertia dominated microjet ejection mode forms the boundary between the low and high frequency modes, f_1 and f_2, respectively, we can associate f_1 at which the drop resonates with the capillary-inertia pinch-off frequency f_i. Balancing capillary and inertia forces, the latter scaling as $\rho_L R_o^2/\mathcal{T}^2$, where $\mathcal{T}$ is the relevant time scale (Chen and Steen, 1997), $f_i \sim$ 10–100 Hz, which is of the same order as f_1.

Drop pinch-off and wetting, conversely, arises due to a negative polarization which gives rise to an oppositely directed force that drives liquid up the needle tip. Figure 4 depicts the real part of the Clausius-Mossotti (Maxwell-Wagner) polarization factor defined in Eq. (1) as a function of the applied frequency. At low frequencies, Re[f_{CM}] is positive but becomes negative at higher frequencies; the reversal occurs at a *crossover frequency* f_c, given by

$$f_c = \frac{1}{2\pi}\left[\frac{(\kappa_o - \kappa_L)(2\kappa_o + \kappa_L)}{(\varepsilon_o - \varepsilon_L)(2\varepsilon_o + \varepsilon_L)}\right]^{\frac{1}{2}}, \qquad (2)$$

from which we estimate $f_c \sim$ 30 kHz. Below f_c, gas-phase or interfacial liquid ionization reaction generates excess negative charges at the interface when the field is in the direction of the needle tip as shown in Fig. 4, resulting in a normal Maxwell stress that acts to stretch the meniscus. Above f_c, there is inadequate time for the reaction to produce sufficient ions. Instead, molecular dipolarization occurs at the interface thereby supplying it with a net positive charge when the field is directed towards the needle tip. This gives rise to equally dominant normal and tangential Maxwell stresses that flattens the drop and forces liquid to wet the side of the needle as depicted in Fig. 4 for high frequencies. The effects do not reverse in the other half of the AC cycle since the direction of the stresses remains identical. In experiments with toluene with a very low conductivity $\kappa_L < 10^{-12}$ S/m, no drop ejection is observed. Instead, electrowetting is dominant at all frequencies which is consistent with our arguments above since the onset boundary for electrowetting at f_c is shifted to 5 kHz for toluene.

The drop can be represented as a parallel resistor-capacitor circuit in the Maxwell-Wagner interfacial polarization mechanism. In this analogy, the interfacial ionization reaction is represented by a Faradaic reaction resistor with resistance R_c and the charge accumulation produced by the ionization reaction is represented by a dielectric capacitor with capacitance C. At low f, the reaction has sufficient time to produce ions and hence there is a large potential drop across the capacitor resulting in the build up of charges giving rise to positive polarization and drop ejection. However, there is insufficient time for reaction to occur at high f and therefore a large potential drop across the resistor is realized resulting in negative polarization and hence wetting.

The equivalent R_cC circuit also consistently predicts the minimum in the critical voltage V_c in Fig. 2. Given that the normal Maxwell stress $\tau_n = PE_n$, where $P = \varepsilon_o \mathrm{Re}[f_{CM}]E_\infty$ is the polarization and E_n is the normal electric field, there exists a optimum frequency corresponding to the R_cC relaxation frequency $f_{RC} \sim 1/R_cC$ at which τ_n is maximum and hence V_c is minimum. This is because reaction charging at low frequencies ($f << f_{RC}$) releases excessive ions that essentially screen the external field whereas insufficient reaction time at high frequencies ($f >> f_{RC}$) result in low polarization of the interface. Moreover, at high frequencies above f_c, the reversal of the polarization results in an oppositely directed Maxwell stress, and hence $f_c \sim f_{RC}$. Since the screening of the external field is minimum and as P is high at V_c, the enhanced transient AC conductivity due to the release of ions by the reaction is negligible and we use the bulk DC liquid conductivity to calculate R_c, which is approximately 2 MΩ in our experiments. C, on the other hand, is roughly 10 pF, and hence $f_{RC} \sim$ 200 kHz, which is consistent with the frequency at V_c observed in Fig. 2. This also suggests a negligible interfacial tangential stress; the meniscus stretching is predominantly driven by the normal stress at the meniscus tip. In addition, both f_c and f_{RC} are also related to the frequency corresponding to the relaxation frequency of the Maxwell-Wagner polarization $f_p \sim (2\kappa_o+\kappa_L)/(2\varepsilon_o+\varepsilon_L) \sim$ 100 kHz. f_p, which is roughly in between the estimates for f_c and f_{RC}, is an approximation for the frequency at which the onset of wetting at f_c completely suppresses drop ejection, i.e. where $f_2 \rightarrow f_1$, as shown in Fig. 3.

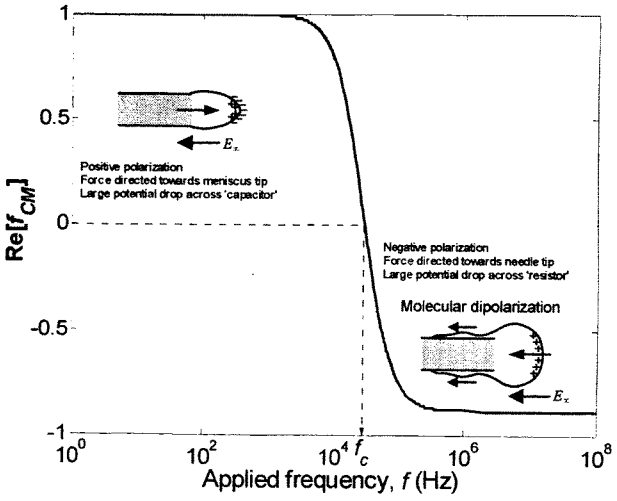

Fig. 4 Real part of the Clausius-Mossotti (Maxwell-Wagner) factor as a function of the applied frequency.

NUMERICAL SIMULATION

Simple lubrication theory is considered to study the dynamics of the stretching meniscus tip under the influence of Maxwell-Wagner stresses. We assume that the meniscus tip, located at the edge of the spherical drop, is already slightly elongated such that it is both slender and axisymmetric, an assumption that will be justified later. An arbitrary position close to the edge of the spherical drop with radius R_o^* is adopted for the origin of the axial coordinate z^*, the asterisk henceforth denoting dimensional quantities. The following transformations are applied to render the problem dimensionless:

$$r \equiv \frac{r^*}{R_{oo}^*}, \quad z \equiv \frac{z^*}{L_o^*}, \quad t \equiv \frac{\gamma_L^*}{\mu_L^* L_o^*} t^*, \quad p \equiv \frac{R_{oo}^*}{\gamma_L^*} p^*, \text{ and, } \quad u \equiv \frac{\mu_L^*}{\gamma_L^*} u^*, \tag{3}$$

where r^* is the radial coordinate, t^* denotes the time, and, p^* and u^* are the pressure and axial velocity of the meniscus film, respectively. R_{oo}^* is the initial interface position of the meniscus tip, taken to be some fraction of R_o^*, and L_o^* is some characteristic macroscopic length scale such that $R_o^* << R_{oo}^* << L_o^*$. It is then possible to write the Navier-Stokes equation of motion in the lubrication limit as

$$\delta \frac{\partial p}{\partial z} = \frac{1}{r} \frac{\partial}{\partial r}\left(r \frac{\partial u}{\partial r} \right), \tag{4}$$

where $\delta \equiv R_{oo}^*/L_o^*$ is a small parameter. It can then be shown from the kinematic jump condition and the boundary conditions $\partial u/\partial r = 0$ at $r = 0$ and $u = 0$ at $r = R$, where $R(z,t)$ is the interfacial meniscus position, that (Yeo and Chang, 2004)

$$\frac{\partial R}{\partial t} = \frac{\delta}{16} \frac{\partial}{\partial z}\left(R^4 \frac{\partial p}{\partial z} \right). \tag{5}$$

For reasons given earlier and since the liquid permittivity far exceeds the gas permittivity, the tip acts as a constant-potential cylindrical surface where the field is predominantly in the normal direction. Nevertheless, despite the absence of tangential Maxwell stresses, we invoke the no-slip boundary condition at the interface since it is likely to be rigid due to the presence of a surface layer arising from interfacial reactions. This rigid layer is necessary to account for the viscous effects observed, and is consistent with our Maxwell-Wagner mechanism that requires a high permittivity and conductivity layer.

In the absence of tangential Maxwell stresses, the far field in the lubrication limit is thus V^*/L_o^* and the field at the interface scales as $1/R$ (Hinch, 1991). Neglecting a unit-order coefficient dependent on the actual drop geometry and taking R_{oo}^* as a convenient macroscopic length scale for the far-field asymptote, the normal interfacial electric field can be approximated by

$$E_n \sim \frac{V^*}{L_o^*} \frac{R_{oo}^*}{R}. \tag{6}$$

From the definition of τ_n above and Eq. (6), the normal stress balance incorporating the normal Maxwell stress, can thus be written in dimensionless form utilizing the scalings described in Eq. (3) as

$$p = \frac{1}{R} - C' \frac{\partial^2 R}{\partial z^2} - \frac{A}{R_2}, \tag{7}$$

where $A \sim 1$–100 and $C' \sim 10^{-4}$–10^{-6} are dimensionless stress and capillary parameters, respectively, defined by

$$A \equiv \frac{\varepsilon_o \mathrm{Re}[f_{CM}] V^{*2} R_{oo}^*}{\gamma_L^* L_o^{*2}}, \text{ and } C' \equiv \frac{\delta^2}{2}. \tag{8}$$

From Eqs. (5) and (7), the final equation governing the evolution of the meniscus tip interface position is

$$\frac{\partial R}{\partial t} = \frac{\delta}{8} \frac{\partial}{\partial z}\left[\left(AR - \frac{R^2}{2} \right) \frac{\partial R}{\partial z} - \frac{C' R^4}{2} \frac{\partial^3 R}{\partial z^3} \right], \tag{9}$$

from which we observe the competing normal capillary and Maxwell stress effects. In addition, we impose the following initial condition for the meniscus height at $t = 0$:

$$R = \frac{1}{2}\left[1 - \tanh\left(\frac{z - \zeta_1}{\zeta_2} \right) \right]. \tag{10}$$

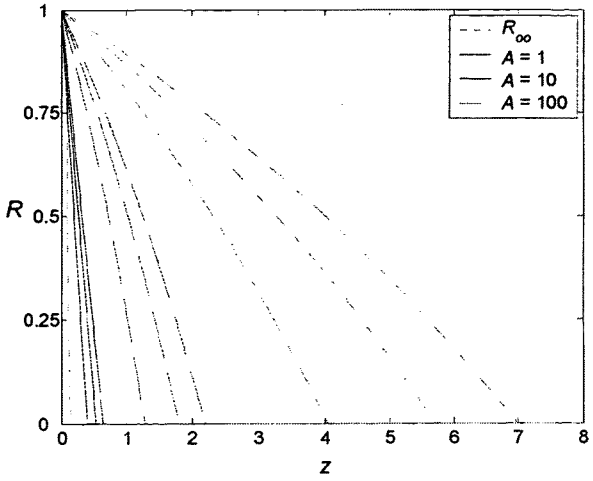

Fig. 5 Evolution profiles showing the stretching of the meniscus tip at t = 50, 100 and 150 for values of A between 1 and 100. Here, $C' = 10^{-4}$. Also shown is the initial profile.

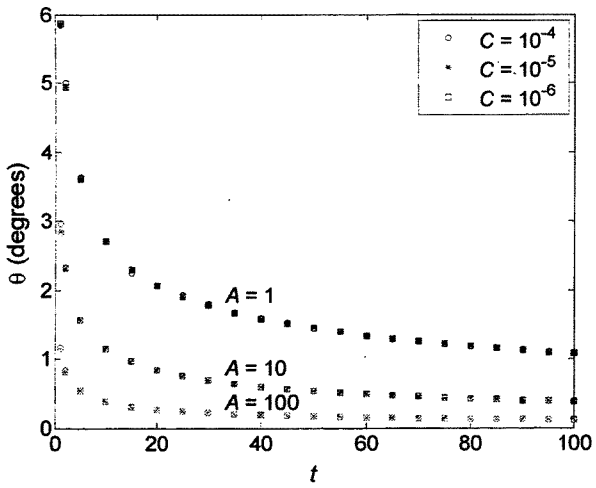

Fig. 6 Temporal variation of the meniscus half angle θ as a function of the system parameters A and C.

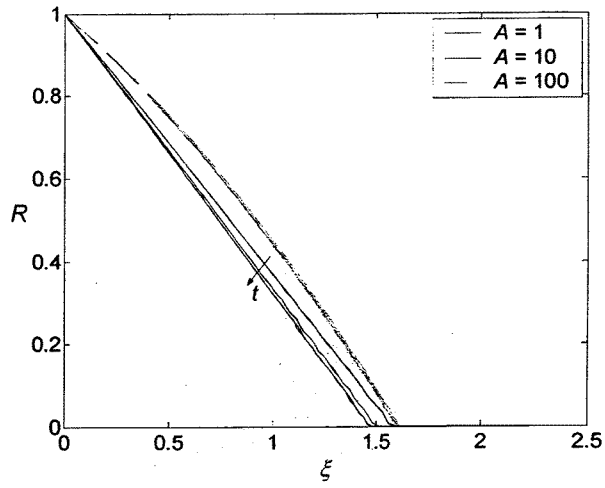

Fig. 7 Advancing meniscus front in transformed variables for t = 50, 100 and 150, and for C = 10^{-4} and 10^{-6}.

The following boundary conditions also apply:

$$\text{At } z = 0,\ R = 1 \quad \text{and} \quad \frac{\partial^3 R}{\partial z^3} = 0, \text{ and,} \tag{11a}$$

$$\text{at } z = z_\infty,\ \frac{\partial R}{\partial z} = 0 \quad \text{and} \quad \frac{\partial^3 R}{\partial z^3} = 0\ , \tag{11b}$$

where z_∞ indicates an axial position far from the region of the meniscus tip. Eq. (9) was solved starting from the initial conditions given in Eq. (10), and subject to boundary conditions given by Eq. (11), using the Method of Lines (Schiesser, 1991). We discretize the spatial derivatives using fourth-order centered differences and Gear's method was used to advance the solution in time. A uniform grid of up to 1000 points was used where convergence was attained by grid refinement. In the simulations, we used the ranges for A and C given above, and, $\zeta_1 = 0.1$ and $\zeta_2 = 0.025$.

Fig. 5 shows the evolution of the meniscus interface with time. The Maxwell stress resulting from the Maxwell-Wagner interfacial polarization can be seen to stretch the meniscus tip into a sharp elongated cone in agreement with the experimental observations. The initial stretching is rapid, as shown by the sharp decrease in the half angle subtended between the meniscus and the horizontal axis θ in Fig. 6, but levels off at later times. Given that the initial stretching rate is not the rate limiting step, the use of a slightly elongated initial profile is justified since the stretching occurs very swiftly upon application of the Maxwell stress. Figure 6 also indicates the dominance of the Maxwell stress over capillary effects at the meniscus tip when $C/A \ll 1$, which is typical of the conditions under which our electrospray is operated. This is also evident in Eq. (7) where the Maxwell stress term demonstrates a higher order singularity than the azimuthal and axial curvature terms at the meniscus tip. This therefore suggests that capillary effects are isolated at the macroscopic bulk of the meniscus where it is observed to cause the meniscus to resonate at some particular frequency.

SELF-SIMILAR DYNAMICS

Since capillary effects are negligible at the meniscus tip compared to the Maxwell stress, we omit both the azimuthal and axial capillary terms from the normal stress balance in Eq. (7) such that the equation governing the meniscus height evolution in Eq. (9) then simplifies to

$$\frac{\partial R}{\partial t} = \frac{\delta A}{8}\frac{\partial}{\partial z}\left(R\frac{\partial R}{\partial z}\right). \tag{12}$$

It is possible to recast the above equation using a self-similar transformation (Jensen and Grotberg, 1992; Yeo et al., 2001) as follows:

$$\xi \equiv \frac{z}{(At)^a}, \quad \tau \equiv t, \text{ and, } R'(\xi,\tau) \equiv R(z,t). \tag{13}$$

We then note that time-dependence of Eq. (12) is removed when $2a - 1 = 0$ or $a = ½$, therefore suggesting that the meniscus front advances as $t^{1/2}$. It can also be shown that the similarity solution for the meniscus height evolution in Eq. (12) is (Yeo and Chang, 2004)

$$R'(\xi,\tau) = \frac{4\xi^2}{3\delta}. \tag{14}$$

Figure 7 depicts the evolution of the meniscus front in light of the similarity scaling above and indicates the $t^{1/2}$ behavior for the dynamics of the advancing meniscus. We note that as long as C/A is small, the profiles collapse onto the $t^{1/2}$ scaling since Eq. (12) retains only the Maxwell stress term with the assumption that A is order 1 or larger. When A is small, however, capillary effects become significant compared to the Maxwell stress and can no longer be omitted.

CONCLUSION

The new high-frequency AC electrospray observed in our experiments reveal a behavior different from that of DC electrosprays. Micron sized drops are ejected periodically from a meniscus that vibrates at a resonant frequency instead of the usual sharp Taylor cone found in DC electrosprays. These drops are larger in dimension and are electroneutral, unlike the smaller drops generated by DC electrospraying where the drops possess a net charge. By using simple scaling arguments, we demonstrate that the stretching of the meniscus occurs due to the stresses that arise from the Maxwell-Wagner interfacial polarization mechanism. At low frequencies, reaction charging due to gas-phase or interfacial ionization dominates resulting in a surface layer of ions, which gives rise to a Maxwell force in the direction of the meniscus tip and acts to stretch it outwards. Above a crossover frequency f_c, the polarization reverses as there is insufficient time for interfacial reaction to occur, resulting in an oppositely directed force, which gives rise to an apparent electrowetting effect that suppresses further drop ejection.

f_c, about which the stretching force is at its maximum, is comparable in magnitude to the frequency associated with the viscous-capillary drop pinch-off time f_v which stipulates the applied frequency at which viscous effects become dominant. Below f_v, viscous forces dominate over inertial forces and hence drop ejection takes place by a tip streaming mechanism. Above f_v, the increasing inertial effects result in the formation of a slender microjet. It is therefore when f_c is close to f_v that microjet formation occurs.

The dynamics of the meniscus tip is studied using lubrication theory. The tip is observed to stretch under the action of the nearly singular normal Maxwell electric stress arising from Maxwell-Wagner interfacial polarization into an elongated cone. We also show that capillary effects are unimportant compared to the Maxwell stress in the vicinity of the meniscus tip for the conditions in our experiments. A self-similar transformation of the equation governing the evolution of the meniscus height demonstrates that the meniscus front advances as $t^{1/2}$.

ACKNOWLEDGEMENTS

The spray data and images in Fig. 2 were taken together with S.-C. Wang. We also acknowledge the support of the Center for Microfluidics and Medical Diagnostics for this work.

NOMENCLATURE

A	Maxwell stress parameter, dimensionless
C	Capacitance, F
C'	Capillary parameter, dimensionless
c	Ionic concentration, M
D	Ionic diffusivity, m^2/s
E_∞	Applied external electric field, V/m
e	Electronic charge, C
F	Force, N
F_γ	Capillary force, N
F_ν	Viscous dissipation force, N
f	Frequency, Hz
f_{CM}	Clausius-Mossotti (Maxwell-Wagner) factor
f_c	Crossover frequency, Hz
f_i	Capillary-inertia drop pinch-off frequency, Hz
f_p	Maxwell-Wagner relaxation frequency, Hz
f_{RC}	R_cC relaxation frequency, Hz
f_v	Viscous-capillary drop pinch-off frequency, Hz
L	Electrode separation, m
L_o	Characteristic length scale, m
N_A	Avogadro constant, $mole^{-1}$
P	Polarization, C/m^2
p	Pressure, dimensionless
Q	Charge, C
R	Meniscus height, dimensionless
R'	Meniscus height in similarity scaling, dimensionless
R_c	Resistance, Ω
R_o	Drop radius, m
R_{oo}	Initial meniscus tip interfacial position, m
r	Radial coordinate, dimensionless
T	Period of applied field, s
T_d	Debye diffusion time scale, s
t	Time, dimensionless
$\mathcal{T}$	Characteristic drop inertia pinch-off time, s
U	Characteristic velocity, m/s
U	Axial velocity, m/s
V	Applied peak-to-peak voltage, V
V_c	Critical voltage for drop ejection, V
z	Axial coordinate, dimensionless
δ	Small parameter, dimensionless
ε	Permittivity, F/m
γ	Interfacial tension, N/m
θ	Meniscus half-angle with horizontal axis, degrees
κ	Conductivity, S/m
λ	Debye layer thickness, m
μ	Viscosity, Pa s
ξ	Axial coordinate in similarity scaling, dimensionless
ρ	Density, kg/m^3
τ	Time in similarity scaling, dimensionless
τ_n	Normal electric field, V/m
ω	Angular frequency, Hz
ζ_1, ζ_2	Initial meniscus shape parameters, dimensionless

Superscripts

*	Dimensional quantity

Subscripts

L	Liquid
o	Ambient
DL	Double layer interfacial polarization
MW	Maxwell-Wagner interfacial polarization

REFERENCES

Borra, J. P., Tombette, Y., and Ehouarn, 1999, Influence of electric field profile and polarity on the mode of EHDA related to electric discharge regimes, *J. Aerosol Sci.*, Vol. 30, pp. 913–925.

Chen, Y.-J., and Steen, P. H., 1997, Dynamics of inviscid capillary breakup: collapse and pinchoff of a film bridge, *J. Fluid Mech.*, Vol. 341, pp. 245–267.

Clopeau, M., and Prunet-Foch, 1991, Electrostatic spraying of liquids: main functioning modes, *J. Electrostatics*, Vol. 25, pp. 165–184.

Eggleton, C. D., Tsai, T.-M., and Stebe, K. J., 2001, Tip streaming from a drop in the presence of surfactants, *Phys. Rev. Lett.*, Vol. 87, 048302.

Fenn, J. B., Mann, M., Meng, C. K., Wong, S. F., and Whitehouse, C. M., 1989, Electrospray ionization for mass spectrometry of large biomolecules, *Science*, Vol. 246, pp. 64–71.

Grace, J. M., and Marijnissen, J. C. M., 1994, A review of liquid atomization by electrical means, *J. Aerosol Sci.*, Vol. 25, pp. 1005–1019.

Hinch, E. J., 1991, *Perturbation methods*, Cambridge University Press, Cambridge.

Jensen, O. E., and Grotberg, J. B., 1992, Insoluble surfactant spreading on a thin viscous film: shock evolution and film rupture, *J. Fluid Mech.*, Vol. 240, pp. 259–288.

Ramos, A., Morgan, H., Green, N. G., and Castellanos, A., 1991, AC electrokinetics: a review of forces in microelectrode structures, *J. Phys. D: Appl. Phys.*, Vol. 31, pp. 2338–2353.

Schiesser, W. E., 1991, *The numerical method of lines*, Academic Press, San Diego.

Yeo, L. Y., and Chang, H.-C., 2004, Self-similar tip stretching and microjet formation in AC electrosprays, submitted to *J. Engineering Math.*

Yeo, L. Y., Lastochkin, D., Wang, S.-C., and Chang, H.-C., 2004, A new AC electrospray mechanism by Maxwell-Wagner polarization and capillary resonance, to appear in *Phys. Rev. Lett.*

Yeo, L. Y., Matar, O. K., Perez de Ortiz, E. S., and Hewitt, G. F., 2001, The dynamics of Marangoni-driven local film drainage between two drops, *J. Colloid Interface Sci.*, Vol. 241, pp. 233–247.